JOURNAL OF GUIDANCE, CONTROL, AND DYNAMICS
Vol. 43, No. 8, August 2020

Hybrid Finite-Frequency Attitude Control Motivated by Volterra Series

Xiaoyu Lang*
Harbin Institute of Technology, 150080 Harbin, People's Republic of China
Christopher J. Damaren†
University of Toronto, Toronto, Ontario M3H 5T6, Canada
and
Xibin Cao‡
Harbin Institute of Technology, 150080 Harbin, People's Republic of China

https://doi.org/10.2514/1.G003856

An analytical solution of Euler's equation is exhibited using the Volterra series theory in the frequency domain. Based on the Volterra series, the nonlinear output frequency response functions of Euler's equation are formulated by a numerical algorithm to reveal an energy-transfer phenomenon. The output responses of Euler's equation have some higher frequency parts than those of the inputs. It provides motivation to design a finite-frequency controller for Euler's equation to accommodate the high-frequency parts of the outputs. A hybrid passive/finite gain control scheme fused with the generalized Kalman–Yakubovich–Popov lemma is used to generate a controller that is effective for stabilizing the angular velocities of Euler's equation. Additionally, quaternions are considered in the proposed hybrid finite-frequency controller to stabilize the attitude of spacecraft. Simulation results are demonstrated to validate the effectiveness of the proposed control schemes.

I. Introduction

THE attitude motion of a rigid-body spacecraft has been described using Euler's equation for a long time. It is a principal dynamic model in spacecraft attitude control problems. Because of mutual-coupled angular velocities, Euler's equation should be categorized as a nonlinear system's differential equation. In approaching this nonlinear system, seeking the solution of Euler's equation would be helpful for analyzing it. One of the analytical solutions of Euler's equation for angular velocities is given in the form of Jacobian elliptic functions in [1]. Another solution for it can be developed using the well-known Runge–Kutta method, which is an iterative method to get approximate solutions of ordinary differential equations. These two solutions, however, are all implemented in the time domain. There is little available literature to discuss the solutions of Euler's equation in the frequency domain. Hence, the frequency domain characteristics of Euler's equation still pose a challenge. In this case, the Volterra series theory is an alternative method to obtain the frequency domain representation of Euler's equation. Primitively, the Volterra series has been used to approximate nonlinear systems such as communication systems [2]. It can capture nonlinearities from input–output dynamics with an infinite sum of multidimensional convolution integrals [3]. This method has been extended to identify the nonlinear dynamic model of aerodynamic systems [4] and aerodynamic output responses [5]. The Volterra series kernels were also developed to predict the frequency behavior of a nonlinear flight system in the time domain [6] and the frequency domain [7]. The Volterra series representation for a nonlinear system with quadratic terms was introduced in [8]. Coincidentally, Euler's equation has quadratic terms with respect to the angular velocities and is assumed to be approximated by the Volterra series in the frequency domain.

For linear systems, the theory of frequency response representations is well developed. It is noted that the frequencies from inputs to outputs in linear systems are identical. In nonlinear systems, output frequency ranges are usually much richer than those of the input. Hence, qualitative analysis is necessary to predict the frequency behaviors of nonlinear systems. As the extension of transfer functions for linear systems, the nonlinear output frequency response functions (NOFRFs) can predict the frequency behaviors of nonlinear systems in a similar manner. To facilitate it, the Volterra series has been used to generate NOFRFs for several nonlinear systems [9–11]. This concept was used in [9] to address the energy-transfer phenomenon in a single-input–single-output (SISO) nonlinear oscillator system in which the output frequency ranges are different from the frequencies of the input excitation. In [10], the NOFRFs were extended to investigate a multi-input–multi-output (MIMO) nonlinear system and its energy transfer in the frequency domain. Therefore, it is assumed that the NOFRFs can also be applicable to predict the nonlinear frequency behavior of Euler's equation in which the energy transfer phenomenon might still exist.

Attitude control is crucial in space missions. As this problem has been discussed in [12], it has become a subject undergoing intense study by many researchers. A number of related control schemes have been proposed in the literature, such as optimal control [13], variable structure control [14], and adaptive control [15]. A strictly positive real (SPR) controller for angular velocities was employed in [16,17] to stabilize a passive spacecraft dynamic system using the passivity theorem as well as the Kalman–Yakubovich–Popov (KYP) lemma. A benefit of the SPR controller is its robustness to modeling errors. However, most of available controllers for spacecraft attitude are mainly built in the time domain rather than the frequency domain. As the fusion of the hybrid passive/finite gain theorem ("hybrid" means that the controller based on this theorem is passive in the low-frequency domain and has finite gain in the high-frequency domain) and the generalized Kalman–Yakubovich–Popov (GKYP) lemma, the controller was developed in [18] to stabilize a single-link manipulator. The GKYP lemma provided a set of schemes to generate controllers at distinctive frequency ranges using linear matrix inequalities (LMIs) [19,20]. It provides motivation to develop a finite-frequency controller using the hybrid passive/finite gain theorem

Received 25 May 2018; revision received 20 March 2020; accepted for publication 23 March 2020; published online 28 April 2020.

*Ph.D. Candidate, Research Center of Satellite Technology, 2 Yikuang Street, Heilongjiang; currently Joint Training Ph.D. Student, Spacecraft Dynamics and Control Laboratory, Institute for Aerospace Studies, University of Toronto, 4925 Dufferin Street, Toronto, Ontario M3H 5T6, Canada.

†Professor, Institute for Aerospace Studies, 4925 Dufferin Street. Associate Fellow AIAA.

‡Professor, Research Center of Satellite Technology, 2 Yikuang Street, Heilongjiang.

with the GKYP lemma to accommodate the possible energy transfer for spacecraft attitude control problems.

This paper first presents the Volterra series frequency representations of Euler's equation. Based on that, the NOFRFs for Euler's equation are established by a numerical algorithm to demonstrate its energy-migration phenomenon. To accommodate this phenomenon, a hybrid finite-frequency strictly passive/finite gain controller for angular velocities based on the GKYP lemma is implemented on Euler's equation. Performance comparison between an SPR controller designed by the KYP lemma and a hybrid frequency controller designed by the GKYP lemma is given. Additionally, quaternions are involved in the hybrid frequency controller for solving the spacecraft attitude control problem. Simulations are shown at the end to demonstrate the effectiveness of the proposed hybrid frequency control schemes.

II. Rotational Dynamics

The attitude motion of a rigid-body spacecraft is governed by Euler's equation [1]

$$\boldsymbol{I}\dot{\boldsymbol{\omega}} + \boldsymbol{\omega}^{\times}\boldsymbol{I}\boldsymbol{\omega} = \boldsymbol{u} \tag{1}$$

where $\boldsymbol{I}$ is the moment of inertia matrix defined in the body frame $\mathcal{F}_b$, $\boldsymbol{\omega} = [\omega_x, \omega_y, \omega_z]^{\top}$ is the angular velocity of the spacecraft, and $\boldsymbol{u} = [u_x, u_y, u_z]^{\top}$ is the total external torque vector applied about the center of the spacecraft. The matrix $\boldsymbol{\omega}^{\times}$ is given by

$$\boldsymbol{\omega}^{\times} = \begin{bmatrix} 0 & -\omega_z & \omega_y \\ \omega_z & 0 & -\omega_x \\ -\omega_y & \omega_x & 0 \end{bmatrix} \tag{2}$$

It is assumed that the moment of inertia matrix

$$\boldsymbol{I} = \begin{bmatrix} I_x & 0 & 0 \\ 0 & I_y & 0 \\ 0 & 0 & I_z \end{bmatrix}$$

is diagonal. Hence, the scalar equations of Eq. (1) become

$$\begin{aligned} I_x\dot{\omega}_x + (I_z - I_y)\omega_y\omega_z &= u_x \\ I_y\dot{\omega}_y + (I_x - I_z)\omega_x\omega_z &= u_y \\ I_z\dot{\omega}_z + (I_y - I_x)\omega_x\omega_y &= u_z \end{aligned} \tag{3}$$

It is noted that Eq. (3) can be written as a quadratic-form state-space equation:

$$\dot{\boldsymbol{x}} = \boldsymbol{A}\boldsymbol{x} + \begin{bmatrix} \boldsymbol{x}^{\top}\boldsymbol{E}_1\boldsymbol{x} \\ \boldsymbol{x}^{\top}\boldsymbol{E}_2\boldsymbol{x} \\ \boldsymbol{x}^{\top}\boldsymbol{E}_3\boldsymbol{x} \end{bmatrix} + \boldsymbol{B}\boldsymbol{u}, \qquad \boldsymbol{y} = \boldsymbol{C}\boldsymbol{x} \tag{4}$$

where $\boldsymbol{x} = [\omega_x, \omega_y, \omega_z]^{\top}$ is the state vector of the system, and

$$\boldsymbol{A} = \boldsymbol{0}_{3\times 3}, \qquad \boldsymbol{B} = \operatorname{diag}\{I_x^{-1}, I_y^{-1}, I_z^{-1}\} \tag{5}$$

Here, the angular velocities are chosen as the outputs of the system; hence $\boldsymbol{C} = \boldsymbol{1}_{3\times 3}$, where $\boldsymbol{1}$ is an identity matrix. The quadratic parameters $\boldsymbol{E}_1$, $\boldsymbol{E}_2$, and $\boldsymbol{E}_3$ are given by

$$\boldsymbol{E}_1 = \begin{bmatrix} 0 & 0 & 0 \\ 0 & 0 & -\frac{I_z - I_y}{2I_x} \\ 0 & -\frac{I_z - I_y}{2I_x} & 0 \end{bmatrix}, \quad \boldsymbol{E}_2 = \begin{bmatrix} 0 & 0 & -\frac{I_x - I_z}{2I_y} \\ 0 & 0 & 0 \\ -\frac{I_x - I_z}{2I_y} & 0 & 0 \end{bmatrix},$$
$$\boldsymbol{E}_3 = \begin{bmatrix} 0 & -\frac{I_y - I_x}{2I_z} & 0 \\ -\frac{I_y - I_x}{2I_z} & 0 & 0 \\ 0 & 0 & 0 \end{bmatrix} \tag{6}$$

There are two different types of solutions of Eq. (3). Generally, a commonly used solution is obtained from the well-known Runge–Kutta method. This solution is usually available for arbitrary control inputs. Based on some special inputs like impulse functions, an analytical solution can be produced for Euler's equation in the form of Jacobian elliptic functions [1]. However, these solutions are all implemented in the time domain instead of the frequency domain. The frequency domain characteristics of Euler's equation cannot be exploited by the above two solutions but might be developed and predicted with the Volterra series.

III. Nonlinear Approximation Based on Volterra Series

In this section, the Volterra series will be used to approximate Euler's equation and yield its analytic solutions in the frequency domain. The simulations of the approximation are conducted to seek the minimal truncation order that can capture the nonlinearity of Euler's equation by the Volterra series.

A. Preliminary for Volterra Series

Consider a general nonlinear system

$$\dot{\boldsymbol{x}} = \boldsymbol{f}(t, \boldsymbol{x}(t), \boldsymbol{u}(t)), \qquad \boldsymbol{y}(t) = \boldsymbol{g}(t, \boldsymbol{x}(t), \boldsymbol{u}(t)) \tag{7}$$

where $\boldsymbol{x} \in \mathcal{R}^n$ is the state vector, $\boldsymbol{u} \in \mathcal{R}^m$ denotes the input vector, and $\boldsymbol{y} \in \mathcal{R}^k$ is the output vector. The functions $\boldsymbol{f}$ and $\boldsymbol{g}$ contain nonlinearities. The input–output relation can be approximated by the theory of Volterra series as

$$\boldsymbol{y}(t) = \sum_{i=1}^{\infty} \int_{-\infty}^{\infty}\int_{-\infty}^{\infty}\cdots\int_{-\infty}^{\infty} h_i(\tau_1, \tau_2, \ldots, \tau_i) \prod_{j=1}^{i} \boldsymbol{u}(t-\tau_j)\,\mathrm{d}\tau_j \tag{8}$$

where $h_i(\tau_1, \tau_2, \ldots, \tau_i)$ is the ith-order Volterra kernel in the time domain. Taking the multidimensional Fourier transform of $h_i(\tau_1, \tau_2, \ldots, \tau_i)$ yields the ith-order Volterra kernel in the frequency domain:

$$\begin{aligned} H_i(\mathrm{j}\omega_1, \ldots, \mathrm{j}\omega_i) = \int_{-\infty}^{\infty}\int_{-\infty}^{\infty}\cdots\int_{-\infty}^{\infty} h_i(\tau_1, \tau_2, \ldots, \tau_i) \\ \times \exp^{-\mathrm{j}(\omega_1\tau_1 + \cdots + \omega_i\tau_i)}\,\mathrm{d}\tau_1 \ldots \mathrm{d}\tau_i \end{aligned} \tag{9}$$

When the complex frequency is denoted by s, Eq. (9) becomes

$$\begin{aligned} H_i(s_1, \ldots, s_i) = \int_{-\infty}^{\infty}\int_{-\infty}^{\infty}\cdots\int_{-\infty}^{\infty} h_i(\tau_1, \tau_2, \ldots, \tau_i) \\ \times \exp^{-(s_1\tau_1 + \cdots + s_i\tau_i)}\mathrm{d}\tau_1 \ldots \mathrm{d}\tau_i \end{aligned} \tag{10}$$

There are several methods to determine the Volterra kernels, such as the canceling-system approach [8] and the growing exponential approach [21,22]. Compared with the growing exponential approach, the canceling-system approach is more intuitive to understand and formulate. Given that Euler's equation is a quadratic MIMO nonlinear state-space equation, the canceling-system approach is easier for getting its Volterra model [8]. The canceling-system approach is

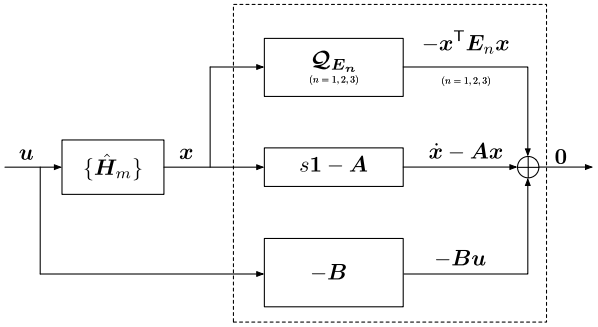

Fig. 1 Canceling-system for $u \to x$.

implemented by building a null system as illustrated in Fig. 1 to determine the Volterra kernel of Euler's equation.

In Fig. 1, the Volterra kernel $\{\hat{\boldsymbol{H}}_m\}$ shows the connection between the input $\boldsymbol{u}$ and the state $\boldsymbol{x}$. Since the output $\boldsymbol{y} = \boldsymbol{C}\boldsymbol{x}$, the Volterra kernel for $\boldsymbol{u} \to \boldsymbol{y}$ becomes $\{\boldsymbol{H}_m\} = \boldsymbol{C}\{\hat{\boldsymbol{H}}_m\}$. In Fig. 1, the right part (dashed line square) includes three branches, which are added together to form a "$\mathbf{0}$" output. It means that Volterra series $\{\hat{\boldsymbol{H}}_m\}$ in the left part is canceled by the right part (dashed line square). Hence, it is named the "canceling-system approach." Based on the method introduced in [8], a brief algorithm is given to facilitate the formulation of Volterra kernels in Algorithm 1.

Algorithm 1: Steps to obtain $\boldsymbol{H}_m(s_1, \ldots, s_m)$ via canceling-system approach [8]

1: Based on Eqs. (A1) and (A3) in the Appendix, the middle branch in the right part (dashed line square) represents the subsystem $\mathcal{S}_{\boldsymbol{u}\mapsto\dot{\boldsymbol{x}}-\boldsymbol{A}\boldsymbol{x}}$ whose corresponding kernel is $[(s_1 + \cdots + s_m)\mathbf{1} - \boldsymbol{A}]\hat{\boldsymbol{H}}_m(s_1, \ldots, s_m)$.

2: Based on Eq. (A2) in Appendix, the top branch of the right part (dashed line square) stands for the quadratic subsystem $\mathcal{S}_{\boldsymbol{u}\mapsto -\boldsymbol{x}^{\top}\boldsymbol{E}_n\boldsymbol{x}}$ $(n = 1, 2, 3)$. Its corresponding kernel is $\sum_{k=1}^{m-1} \hat{\boldsymbol{H}}_k(s_1, \ldots, s_k)^{\top}\boldsymbol{E}_n\hat{\boldsymbol{H}}_{m-k}(s_{k+1}, \ldots, s_m)$ $(n = 1, 2, 3)$.

3: The inferior branch indicates the subsystem $\mathcal{S}_{\boldsymbol{u}\mapsto\boldsymbol{B}\boldsymbol{u}}$. Its corresponding kernel is $\boldsymbol{B}$ for $m = 1$ and $\mathbf{0}$ for $m \geq 2$, as $\mathcal{S}_{\boldsymbol{u}\mapsto\boldsymbol{B}\boldsymbol{u}}$ has no explicit dependence on $\boldsymbol{x}$.

4: Adding all kernels of the three branches and following Eq. (A1), the Volterra kernel matrices $\boldsymbol{H}_m(s_1, \ldots, s_m)$ of Euler's equation are given as Eqs. (11–13).

$$\boldsymbol{H}_m = \boldsymbol{C}\hat{\boldsymbol{H}}_m,$$

$$\hat{\boldsymbol{H}}_m(s_1, \ldots, s_m) = [(s_1 + \cdots + s_m)\mathbf{1} - \boldsymbol{A}]^{-1}\boldsymbol{J}_m(s_1, \ldots, s_m) \tag{11}$$

$$\boldsymbol{J}_1(s_1) = \boldsymbol{B} \qquad (m = 1) \tag{12}$$

$$\boldsymbol{J}_m(s_1, \ldots, s_m) = \sum_{k=1}^{m-1} \begin{bmatrix} \hat{\boldsymbol{H}}_k(s_1, \ldots, s_k)^{\top}\boldsymbol{E}_1\hat{\boldsymbol{H}}_{m-k}(s_{k+1}, \ldots, s_m) \\ \hat{\boldsymbol{H}}_k(s_1, \ldots, s_k)^{\top}\boldsymbol{E}_2\hat{\boldsymbol{H}}_{m-k}(s_{k+1}, \ldots, s_m) \\ \hat{\boldsymbol{H}}_k(s_1, \ldots, s_k)^{\top}\boldsymbol{E}_3\hat{\boldsymbol{H}}_{m-k}(s_{k+1}, \ldots, s_m) \end{bmatrix} \quad (m \geq 2) \tag{13}$$

B. Simulation of Euler's Equation Using Volterra Series

The Volterra series for Euler's equation in Eqs. (3–6) is now studied using the canceling-system approach. The realization of the Volterra model of Euler's equation is implemented using the MATLAB/Simulink with the instruction provided in [8]. The simulation parameters are set as follows: the moment of inertia $\boldsymbol{I} = \text{diag}\{15, 50, 35\}$ kg · m^2 and the initial angular velocity $\boldsymbol{\omega}_0 = [0.15, 0.15, 0.15]^{\top}$ rad/s. Before demonstrating the simulation results, the convergence condition of the Volterra series for a MIMO quadratic nonlinear system is worth discussing. The convergence condition stated in [8] is $\max\{Re(\lambda\{\boldsymbol{A}\})\} < 0$, where $\lambda\{\boldsymbol{A}\}$ denotes the eigenvalues of the matrix $\boldsymbol{A}$. To satisfy this condition, an equivalent form is used by adding a term $\boldsymbol{I}\boldsymbol{\omega}$ to the right-hand side of Eq. (1) and then subtracting it at the end as

$$\boldsymbol{I}\dot{\boldsymbol{\omega}} = -\boldsymbol{I}\boldsymbol{\omega} - \boldsymbol{\omega}^{\times}\boldsymbol{I}\boldsymbol{\omega} + \boldsymbol{u} + \boldsymbol{I}\boldsymbol{\omega} \tag{14}$$

Taking the special derivations, the matrix $\boldsymbol{A}$ in Eq. (4) becomes $\boldsymbol{A} = -\mathbf{1}_{3\times 3}$.

Figure 2 exhibits the time response of angular velocities using the Runge–Kutta method, linear-based model, the second-order Volterra models, and the third-order ones, respectively, when the input is of the form $\boldsymbol{u} = A_u \sin(\omega_u t) \cdot [1, 1, 1]^{\top}$ with $A_u = 1$, $\omega_u = 1$ rad/s. From the simulation results, it is explicit that the third-order Volterra series can capture the nonlinearity of Euler's equation accurately. The truncation order of the Volterra series at $N = 3$ will be used in the next section.

IV. Nonlinear Output Frequency Response Functions for Euler's Equation with Volterra Series

A dominant characteristic of a linear system's frequency response is that the frequencies of the input and output signals remain identical. This feature cannot be simply extended to the nonlinear case. For a nonlinear system, as it was developed in [9], the output frequencies are different from those for the inputs, which is the so-called energy transfer. In this section, the energy transfer from inputs to outputs in Euler's equation will be studied.

A. Energy Transfer Properties of Euler's Equation in the Frequency Domain

Consider the scalar equations of Euler's equation as shown in Eq. (3). The moment of inertia $\boldsymbol{I}$ is set as the same value as them used in the simulation in the last section. The input signals are changed to

$$u_1 = \frac{\sin(t) - \sin(0.7t)}{t}, \qquad u_2 = \frac{\sin(0.7t) - \sin(0.3t)}{t},$$
$$u_3 = \frac{\sin(0.3t) - \sin(0.1t)}{t} \tag{15}$$

The numerical simulations for Eq. (3) are performed when the input signals in Eq. (15) are used. The vector $\boldsymbol{Y} = [Y_1, Y_2, Y_3]^{\top}$ denotes the Fourier transform of the output $\boldsymbol{y} = [y_1, y_2, y_3]^{\top}$ specified in Eq. (4). The frequency ranges of the inputs signals u_1, u_2, and u_3 are set as $[0.7, 1]$, $[0.3, 0.7]$, and $[0.1, 0.3]$ rad/s, respectively. Figure 3 shows the spectra of the input signals. Figure 4 depicts the spectra of the output $\boldsymbol{y}$. It is noted that some energy migrates beyond the upper bound of the input frequency range (1 rad/s). A further interpretation of this phenomenon will be made from the theory of the NOFRFs in the next subsection.

B. NOFRFs for MIMO Volterra Series Model

For linear systems, the frequency domain analysis plays a dominant role in the design of controllers. The characteristics of linear systems can be clearly demonstrated using the frequency response function $H(\text{j}\omega)$. If $U(\text{j}\omega)$ and $Y(\text{j}\omega)$ are assumed to denote the spectrum of a linear system's time responses of inputs $u(t)$ and outputs $y(t)$ respectively, the relation between input spectrum and output spectrum can be expressed by

$$Y(\text{j}\omega) = H(\text{j}\omega)U(\text{j}\omega) \tag{16}$$

Considering the nonlinear system in Eq. (7), its Volterra series model in the time domain is given by Eq. (8). The analogous definition of the output frequency response in Eq. (8) has been provided in [23] based on the theory of Volterra series in the frequency domain:

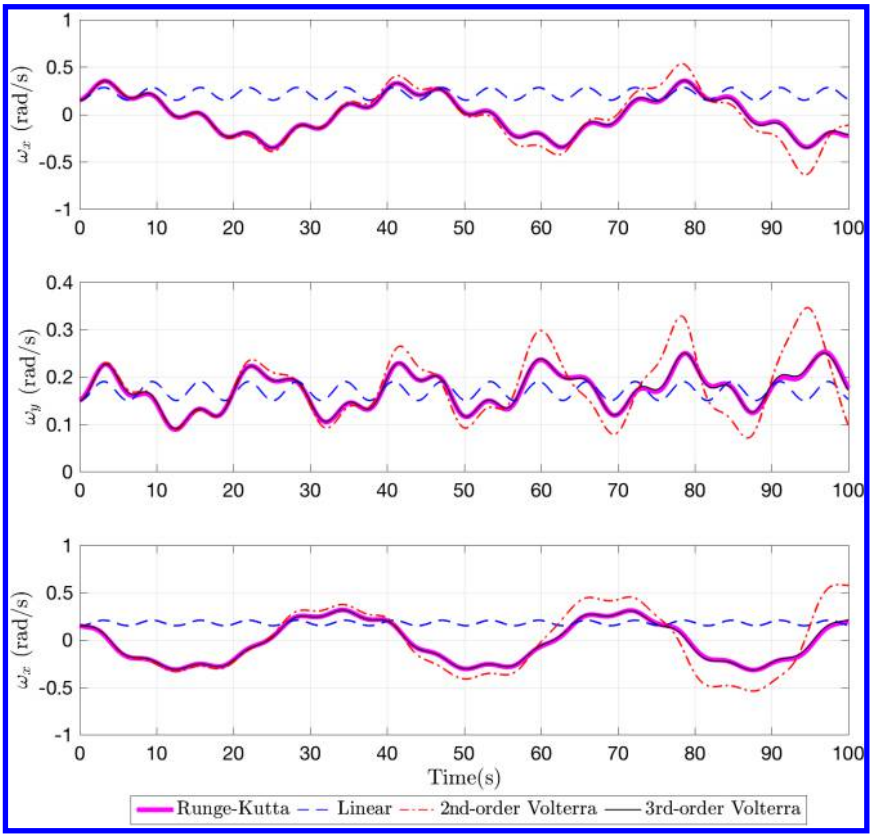

Fig. 2 Time response for angular velocities.

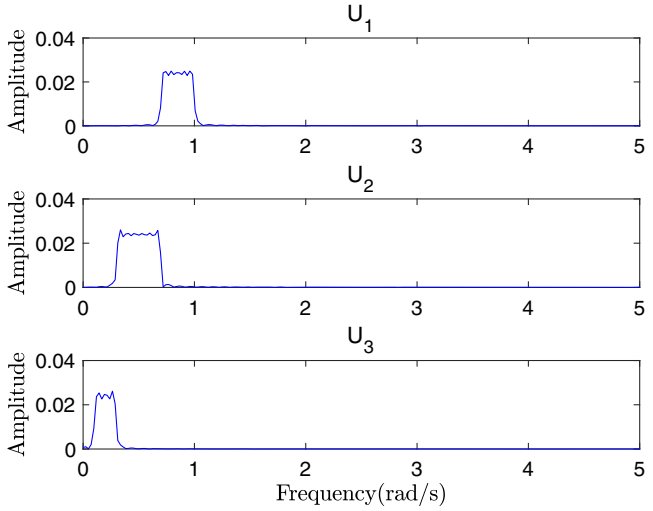

Fig. 3 Spectra of input signals.

$$Y(\mathrm{j}\omega) = \sum_{i=1}^{N} Y^{(i)}(\mathrm{j}\omega),$$

$$Y^{(i)}(\mathrm{j}\omega) = \frac{1}{(2\pi)^{i-1}\sqrt{i}} \int_{\omega_1+\cdots+\omega_i=\omega} H_i(\mathrm{j}\omega_1,\ldots,\mathrm{j}\omega_i) \prod_{j=1}^{i} U(\mathrm{j}\omega_j)\,\mathrm{d}\sigma_{i\omega} \tag{17}$$

where N is the maximum order of the system nonlinearity, $Y_i(\mathrm{j}\omega)$ denotes the ith order of the output frequency response, $\int_{\omega_1+\cdots+\omega_i=\omega}(*)\,\mathrm{d}\sigma_{i\omega}$ is the integration of $(*)$ over the hyperplane $\omega_1+\cdots+\omega_i=\omega$, and $H_i(\mathrm{j}\omega_1,\ldots,\mathrm{j}\omega_i)$ has the same form as Eq. (9). Based on the above results, the definition of nonlinear output frequency response function $G^{(i)}(\mathrm{j}\omega)$ was introduced in [9] as

$$G^{(i)}(\mathrm{j}\omega) = \frac{\int_{\omega_1+\cdots+\omega_i=\omega} H_i(\mathrm{j}\omega_1,\ldots,\mathrm{j}\omega_i)\prod_{j=1}^{i} U(\mathrm{j}\omega_j)\,\mathrm{d}\sigma_{i\omega}}{\int_{\omega_1+\cdots+\omega_i=\omega}\prod_{j=1}^{i} U(\mathrm{j}\omega_j)\,\mathrm{d}\sigma_{i\omega}} \tag{18}$$

where

$$U^{(i)}(\mathrm{j}\omega) = \int_{\omega_1+\cdots+\omega_i=\omega} \prod_{j=1}^{i} U(\mathrm{j}\omega_j)\,\mathrm{d}\sigma_{i\omega} \neq 0 \tag{19}$$

Hence, the output frequency response in Eq. (17) is equivalent to

$$Y(\mathrm{j}\omega) = \sum_{i=1}^{N} G^{(i)}(\mathrm{j}\omega)U^{(i)}(\mathrm{j}\omega) \tag{20}$$

This input–output relation in the frequency domain for nonlinear system is illustrated in Fig. 5 to compare with its linear counterpart [10]. Note that the NOFRFs $G^{(1)}(\mathrm{j}\omega), G^{(2)}(\mathrm{j}\omega),\ldots$ represent the frequency domain gains for the higher moments of the frequency domain inputs.

Euler's equations have three inputs and three outputs, which are $\boldsymbol{u} = [u_1, u_2, u_3]^\mathrm{T}$ and $\boldsymbol{y} = [y_1, y_2, y_3]^\mathrm{T}$ in the time domain and $\boldsymbol{U} = [U_1, U_2, U_3]^\mathrm{T}$ and $\boldsymbol{Y} = [Y_1, Y_2, Y_3]^\mathrm{T}$ in the frequency domain. As an extension of the SISO case shown in Eqs. (16–20), the MIMO Volterra series approximation applied to the pth output of Euler's equation in [10] is given by

$$\begin{aligned} Y_p(\mathrm{j}\omega) = &\sum_{k_1=1}^{3} G^{(1)}_{p,k_1}(\mathrm{j}\omega)[U_{k_1}(\mathrm{j}\omega)] \\ &+ \sum_{k_1=1}^{3}\sum_{k_2=k_1}^{3} G^{(2)}_{p,k_1k_2}(\mathrm{j}\omega)[U_{k_1}(\mathrm{j}\omega)U_{k_2}(\mathrm{j}\omega)]\cdots \\ &+ \sum_{k_1=1}^{3}\cdots\sum_{k_3=k_2}^{3} G^{(N)}_{p,k_1\cdots k_N}(\mathrm{j}\omega)[U_{k_1}(\mathrm{j}\omega)\cdots U_{k_N}(\mathrm{j}\omega)] \end{aligned} \tag{21}$$

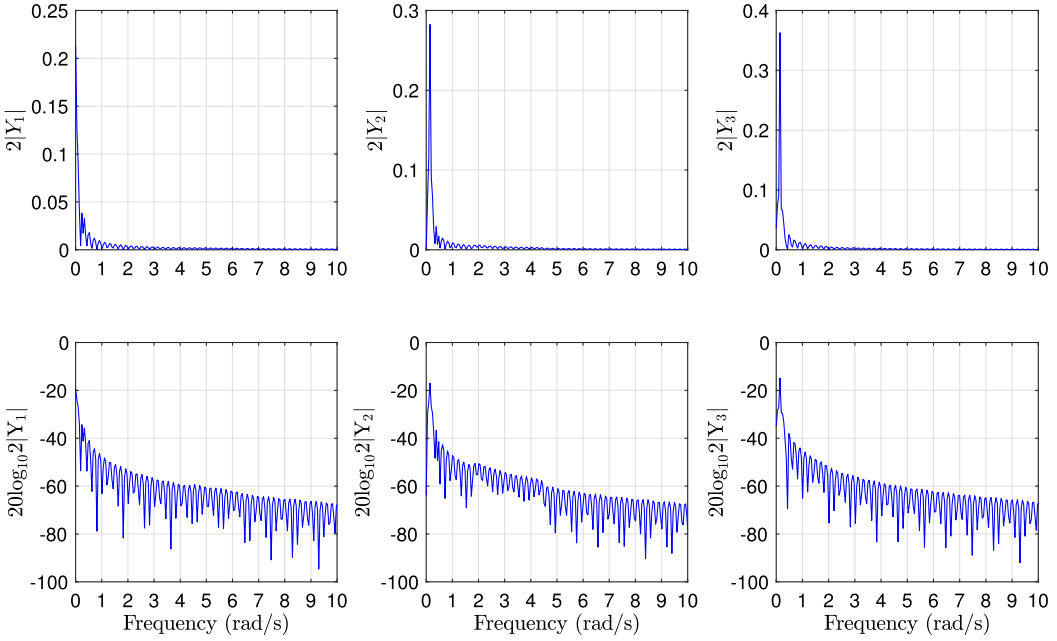

Fig. 4 Spectrum of *y*.

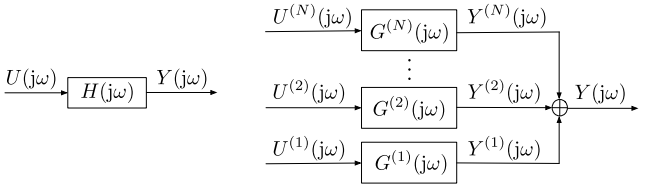

a) Linear **b) Nonlinear**

Fig. 5 Input–output relation in the frequency domain for a) linear system b) nonlinear system.

where the term $G^{(i)}_{p,k_1k_2\ldots k_N}$ $(k_1+k_2+\cdots+k_N=i,$ $i=1,2,\ldots,N)$ denotes ith-order NOFRFs and N is set as the same truncated order as the Volterra kernel from Sec. III.B (which was set as $N=3$). The subscript of $G^{(i)}_{p,k_1k_2\ldots k_N}$ generally denotes

$$G^{(n)}_{p,\underbrace{1\ \cdots\ 1}_{N_1}\underbrace{2\ \cdots\ 2}_{N_2}\underbrace{3\ \cdots\ 3}_{N_3}}(\mathrm{j}\omega)=G^{(n)}_{(p,P_1=N_1,P_2=N_2,P_3=N_3)} \tag{22}$$

where $N_m(m=1,2,3)$ represents the N_mth input involved into this system. According to the formula [Eq. (35) in Ref. [10]], in Euler's equation's case, the number of terms contained in Eq. (21) is 19. Specifically, the 19-term pth-order NOFRFs $\{G_p\}$ include $G^{(1)}_{(p,100)}$, $G^{(1)}_{(p,010)}$, $G^{(1)}_{(p,001)}$, $G^{(2)}_{(p,200)}$, $G^{(2)}_{(p,020)}$, $G^{(2)}_{(p,002)}$, $G^{(2)}_{(p,110)}$, $G^{(2)}_{(p,011)}$, $G^{(2)}_{(p,101)}$, $G^{(3)}_{(p,300)}$, $G^{(3)}_{(p,030)}$, $G^{(3)}_{(p,003)}$, $G^{(3)}_{(p,120)}$, $G^{(3)}_{(p,210)}$, $G^{(3)}_{(p,012)}$, $G^{(3)}_{(p,021)}$, $G^{(3)}_{(p,102)}$, $G^{(3)}_{(p,201)}$, and $G^{(3)}_{(p,111)}$.

For the input frequency-domain form $U_{k_n}(n=1,2,\ldots,N)$,

$$\begin{aligned}&[U_{k_1}(\mathrm{j}\omega)\ \cdots\ U_{k_N}(\mathrm{j}\omega)]\\&=[\underbrace{U_1(\mathrm{j}\omega)\ \cdots\ U_1(\mathrm{j}\omega)}_{N_1}\times\cdots\times\underbrace{U_3(\mathrm{j}\omega)\ \cdots\ U_3(\mathrm{j}\omega)}_{N_3}]\end{aligned} \tag{23}$$

Hence, Eq. (21) is of the form

$$\begin{aligned}Y_p(\mathrm{j}\omega)=[&U_1,U_2,U_3,U_1^2,U_2^2,U_3^2,U_1U_2,U_2U_3,U_1U_3,U_1^3,U_2^3,U_3^3,\\&U_1U_2^2,U_1^2U_2,U_2U_3^2,U_2^2U_3,U_1U_3^2,U_1^2U_3,U_1U_2U_3][G_p]\end{aligned} \tag{24}$$

where

$$[G_p]=[\underbrace{G^{(1)}_{(p,100)}\ \cdots\ G^{(3)}_{(p,111)}}_{\text{19-term NOFRFs}}]^{\mathrm{T}} \tag{25}$$

Assuming that Euler's equations are excited by the input signals $\tilde{u}_i(t)=\alpha u_i(t)$ $(i=1,2,3)$, the corresponding frequency-domain forms are $\tilde{U}_i(\mathrm{j}\omega)=\alpha U_i(\mathrm{j}\omega)$, $i=1,2,3$. Substituting these new input signals into Eq. (24), we can have

$$\begin{aligned}\tilde{Y}_p(\mathrm{j}\omega)=[&\alpha U_1,\alpha U_2,\alpha U_3,\alpha^2U_1^2,\alpha^2U_2^2,\alpha^2U_3^2,\alpha^2U_1U_2,\alpha^2U_2U_3,\\&\alpha^2U_1U_3,\alpha^3U_1^3,\alpha^3U_2^3,\alpha^3U_3^3,\alpha^3U_1U_2^2,\alpha^3U_1^2U_2,\alpha^3U_2U_3^2,\\&\alpha^3U_2^2U_3,\alpha^3U_1U_3^2,\alpha^3U_1^2U_3,\alpha^3U_1U_2U_3][G_p]\end{aligned} \tag{26}$$

To formulate the NOFRFs $[G_p]$, Euler's equation should be excited by different sets of $\tilde{u}_i(t)=\alpha_q u_i(t)(i=1,2,3$ and $q=1,2,\ldots)$. This number of q can also be calculated from [10]. As a result, there are different output frequency responses $\boldsymbol{\mathcal{Y}}_p(\mathrm{j}\omega)=\mathrm{col}\{Y_p^{(q)}(\mathrm{j}\omega)\}(q=1,2,\ldots)$ given by

$$\begin{bmatrix}Y_p^{(1)}(\mathrm{j}\omega)\\Y_p^{(2)}(\mathrm{j}\omega)\\\vdots\\Y_p^{(q)}(\mathrm{j}\omega)\end{bmatrix}=\begin{bmatrix}\alpha_1U_1&\cdots&\alpha_1U_3&\cdots&\alpha_1^3U_1^3&\cdots&\alpha_1^3U_1U_2U_3\\\alpha_2U_1&\cdots&\alpha_2U_3&\cdots&\alpha_2^3U_1^3&\cdots&\alpha_2^3U_1U_2U_3\\\vdots&\vdots&\vdots&\vdots&\vdots&\vdots&\vdots\\\alpha_qU_1&\cdots&\alpha_qU_3&\cdots&\alpha_q^3U_1^3&\cdots&\alpha_q^3U_1U_2U_3\end{bmatrix}[G_p] \tag{27}$$

After defining

$$\boldsymbol{\mathcal{A}}=\begin{bmatrix}\alpha_1U_1&\cdots&\alpha_1U_3&\cdots&\alpha_1^3U_1^3&\cdots&\alpha_1^3U_1U_2U_3\\\alpha_2U_1&\cdots&\alpha_2U_3&\cdots&\alpha_2^3U_1^3&\cdots&\alpha_2^3U_1U_2U_3\\\vdots&\vdots&\vdots&\vdots&\vdots&\vdots&\vdots\\\alpha_qU_1&\cdots&\alpha_qU_3&\cdots&\alpha_q^3U_1^3&\cdots&\alpha_q^3U_1U_2U_3\end{bmatrix} \tag{28}$$

Equation (27) can be written as

$$\mathcal{Y}_p(\mathrm{j}\omega) = \mathcal{A}[G_p] \tag{29}$$

Finally, the pth-order NOFRFs $[G_p]$ are given by

$$[G_p] = [\mathcal{A}^{\top}\mathcal{A}]^{-1}\mathcal{A}^{\top}\mathcal{Y}_p(\mathrm{j}\omega) \tag{30}$$

C. Simulation for NOFRFs of Euler's Equation

The point of exploiting the NOFRFs of Euler's equation is to explain the energy-transfer phenomenon illustrated in Figs. 3 and 4. All parameters for simulations are the same as the last subsection. In Eq. (26), the cross-product terms $U_1^2, U_2^2, U_3^2, U_1U_2, U_2U_3, U_1U_3, U_1^3, U_2^3, U_3^3, U_1U_2^2, U_1^2U_2, U_2U_3^2, U_2^2U_3, U_1U_3^2, U_1^2U_3$, and $U_1U_2U_3$ are likely to be the source of high-frequency components while the frequency ranges of U_1, U_2, U_3 are all less than 1 rad/s. Some of the cross-product terms are shown in Fig. 6. Following the numerical algorithm, some of the amplitudes of NOFRFs $\{G_p\}$ are illustrated in Fig. 7.

From these simulation results, the energy-transfer phenomenon exists in all three orders of NOFRFs. In the low-frequency domain, some responses still remain because all the frequency ranges of input signals are less than 1 rad/s. However, there are still some responses beyond 1 rad/s. Accommodation of the response existing at the higher frequency range is the motivation for the next section.

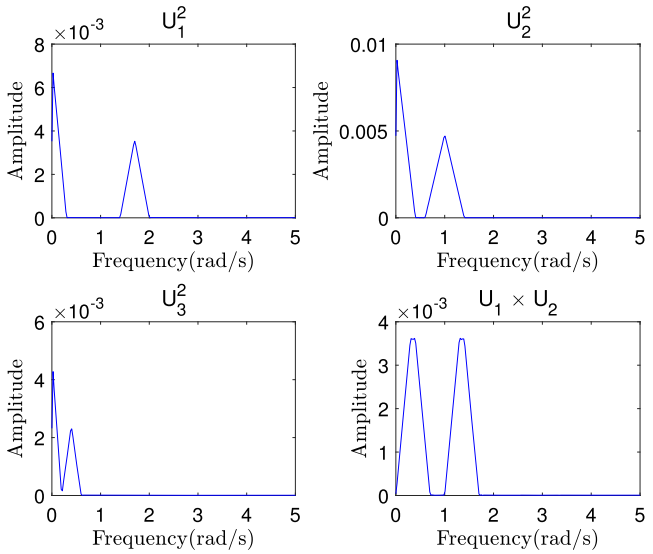

Fig. 6 Spectra of U_1^2, U_2^2, U_3^2, and U_1U_2.

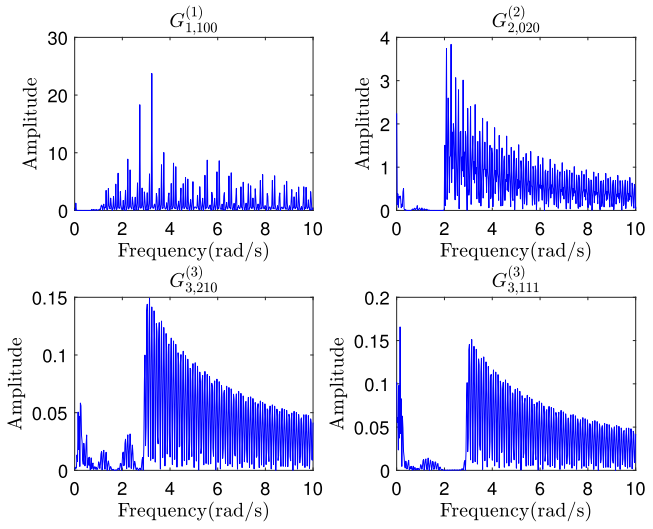

Fig. 7 $|G^{(1)}_{1,100}(\mathrm{j}\omega)|$, $|G^{(2)}_{2,020}(\mathrm{j}\omega)|$, $|G^{(3)}_{3,210}(\mathrm{j}\omega)|$, and $|G^{(3)}_{3,111}(\mathrm{j}\omega)|$.

Remark 1: The order N of NOFRFs in Eq. (17) is a crucial parameter to predict the frequency behaviors of a nonlinear system. However, there have been few guidelines available about the selection of this parameter N. Since the NOFRFs approach is extended from the Volterra series, we use $N = 3$, which is the minimal truncated order to capture the nonlinearity of Euler's equation.

V. Hybrid Frequency Control for Euler's Equation

From the simulation results of the NOFRFs, some frequency responses migrate to the high-frequency domain when the input signals are in the low-frequency range. This motivates that a controller can be designed based on the distinctive frequency domain properties of Euler's equation. In this section, Euler's equation with a prewrap term will be shown to have finite gain. Then, the hybrid passive/finite gain theorem is implemented to design a controller that can maintain passivity (and high gain) in the low-frequency domain and have finite small gain in the high-frequency ranges, and thus attenuate the frequency response migration. Note that NOFRFs were used to illuminate the energy migration to higher frequency but will not be used as a model for controller design. Our controller design will use a linear model of the attitude dynamics (and kinematics), but the energy migration phenomenon motivates gain reduction at higher frequency.

A. Preliminary

For the sake of clarity, the notation $\boldsymbol{y}(\mathrm{j}\omega)$ represents the Fourier transform of a time-domain function $\boldsymbol{y}(t)$. Recall the concepts of $\mathcal{L}_2$ space and its extension $\mathcal{L}_{2e}$, namely, $\boldsymbol{y}(t) \in \mathcal{L}_2$ when $\sqrt{\int_0^\infty \boldsymbol{y}^{\top}(t)\boldsymbol{y}(t)\,\mathrm{d}t} < \infty$ and $\boldsymbol{y}(t) \in \mathcal{L}_{2e}$ when $\sqrt{\int_0^\infty \boldsymbol{y}_T^{\top}(t)\boldsymbol{y}_T(t)\,\mathrm{d}t} < \infty$, $0 \le T < \infty$ ($\boldsymbol{y}_T(t) = \boldsymbol{y}(t), \boldsymbol{0} \le t \le T$ and $\boldsymbol{y}_T = \boldsymbol{0}, t > T$). According to Parseval's theorem [24], one can write $\int_0^\infty \boldsymbol{y}^{\top}(t)\boldsymbol{y}(t)\,\mathrm{d}t = 1/(2\pi)Re\int_{-\infty}^{\infty}\boldsymbol{y}^{\mathrm{H}}(\mathrm{j}\omega)\boldsymbol{y}(\mathrm{j}\omega)\,\mathrm{d}\omega$.

For a general system $\boldsymbol{y} = \mathcal{G}\boldsymbol{e}$ with the operator $\mathcal{G}$: $\mathcal{L}_{2e} \to \mathcal{L}_{2e}$, the input $\boldsymbol{e} \in \mathcal{L}_{2e}$, and the output $\boldsymbol{y} \in \mathcal{L}_{2e}$, a hybrid passive/finite gain system $\mathcal{G}$ is defined in [25] as satisfying

$$\frac{1}{2\pi}\int_{-\infty}^{\infty}\boldsymbol{y}_T^{\mathrm{H}}(\mathrm{j}\omega)\boldsymbol{Q}(\omega)\boldsymbol{y}_T(\mathrm{j}\omega)\,\mathrm{d}\omega + \frac{1}{\pi}Re\int_{-\infty}^{\infty}\boldsymbol{y}_T^{\mathrm{H}}(\mathrm{j}\omega)\boldsymbol{S}(\omega)\boldsymbol{e}_T(\mathrm{j}\omega)\,\mathrm{d}\omega + \frac{1}{2\pi}\int_{-\infty}^{\infty}\boldsymbol{e}_T^{\mathrm{H}}(\mathrm{j}\omega)\boldsymbol{R}(\omega)\boldsymbol{e}_T(\mathrm{j}\omega)\,\mathrm{d}\omega \ge 0 \tag{31}$$

where

$$\boldsymbol{Q}(\omega) = -[\epsilon\alpha(\omega) + \gamma^{-1}(1-\alpha(\omega))]\boldsymbol{1}, \qquad \boldsymbol{S}(\omega) = \frac{1}{2}\alpha(\omega)\boldsymbol{1},$$
$$\boldsymbol{R}(\omega) = [\gamma(1-\alpha(\omega)-\delta\alpha(\omega)]\boldsymbol{1} \tag{32}$$

The passivity of the system $\mathcal{G}$ is revealed by the constant parameters δ and ϵ, and the finite-gain property of the system $\mathcal{G}$ determines γ. The frequency variable α is given by

$$\alpha(\omega) = \begin{cases} 1, & -\omega_c \le \omega \le \omega_c \quad \text{(passive region)} \\ 0, & |\omega| > \omega_c \quad \text{(finite gain region)} \end{cases} \tag{33}$$

where ω_c is the critical frequency. The entire frequency range can be split into two subranges by ω_c. By considering the passive region ($\alpha(\omega) = 1$) and the finite-gain region ($\alpha(\omega) = 0$), Eq. (31) can be satisfied if

$$\frac{1}{2\pi}Re\int_{-\omega_c}^{\omega_c}\boldsymbol{y}_T^{\mathrm{H}}(\mathrm{j}\omega)\boldsymbol{e}_T(\mathrm{j}\omega)\,\mathrm{d}\omega \ge \frac{\epsilon}{2\pi}\int_{-\omega_c}^{\omega_c}\boldsymbol{y}_T^{\mathrm{H}}(\mathrm{j}\omega)\boldsymbol{y}_T(\mathrm{j}\omega)\,\mathrm{d}\omega + \frac{\delta}{2\pi}\int_{-\omega_c}^{\omega_c}\boldsymbol{e}_T^{\mathrm{H}}(\mathrm{j}\omega)\boldsymbol{e}_T(\mathrm{j}\omega)\,\mathrm{d}\omega \tag{34}$$

and

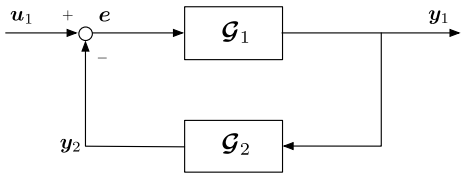

Fig. 8 A negative feedback system.

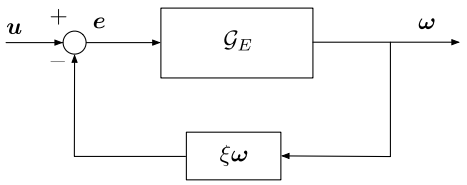

Fig. 9 Euler's equation with the prewrap term.

$$\frac{1}{\pi\gamma}\int_{\omega_c}^{\infty} \boldsymbol{y}_T^{\mathrm{H}}(\mathrm{j}\omega)\boldsymbol{y}_T(\mathrm{j}\omega)\,\mathrm{d}\omega \le \frac{\gamma}{\pi}\int_{\omega_c}^{\infty} \boldsymbol{e}_T^{\mathrm{H}}(\mathrm{j}\omega)\boldsymbol{e}_T(\mathrm{j}\omega)\,\mathrm{d}\omega \tag{35}$$

We say that the system is a hybrid passive/finite-gain system.

Consider the two hybrid passive/finite-gain systems $\mathcal{G}_1: \mathcal{L}_{2e} \to \mathcal{L}_{2e}$ and $\mathcal{G}_2: \mathcal{L}_{2e} \to \mathcal{L}_{2e}$ interconnected with negative feedback as illustrated in Fig. 8.

The stability of these two interconnected negative feedback systems can be guaranteed by the hybrid passivity/finite-gain theorem [25] as follows.

Theorem 1 (hybrid passivity/finite gain theorem): Assume these two systems are hybrid passivity/finite gain systems with corresponding parameters as $\mathcal{G}_1: \delta_1, \epsilon_1, \gamma_1$ and $\mathcal{G}_2: \delta_2, \epsilon_2, \gamma_2$ satisfying Eqs. (34) and (35). The interconnected system with $\mathcal{G}_1$ and $\mathcal{G}_2$ is $\mathcal{L}_2$ stable if $\delta_1 + \epsilon_2 > 0$, $\delta_2 + \epsilon_1 > 0$, and $\gamma_1\gamma_2 < 1$.

For a proof, see [25].

Remark 2: Note that, in particular, a linear controller $\mathcal{G}_2$ with $\delta_2 > 0$, $\epsilon_2 > 0$, and small γ_2 designed using a linear model of the plant $\mathcal{G}_1$ can stabilize a nonlinear system $\mathcal{G}_1$ with $\delta_1 > 0, \epsilon_1 > 0$, and $\gamma_2 < 1/\gamma_1$. We are particularly motivated by the use of a small value of γ_2 to accomplish high-frequency gain reduction.

B. Finite Gain for Euler's Equation with a Prewrap Term

A crucial prerequisite of the hybrid passivity/finite gain theorem is that the plant system should have finite gain. Thus, it is impossible to apply the hybrid passivity/finite gain theorem directly to Euler's equation, because it does not have finite gain. However, it becomes possible when a prewrap term is added into Euler's equation. Before demonstrating the finite-gain nature, a lemma is given at first to show that the mapping $\mathcal{G}_E$ of Euler's equation shown in Eq. (1) from the input $\boldsymbol{u}$ to the angular velocity $\boldsymbol{\omega}$ is passive.

Lemma 1: $\mathcal{G}_E: \boldsymbol{u} \to \boldsymbol{\omega}$ is passive.

Proof: Consider Euler's equation shown in Eq. (1). Its kinetic energy is $H(t) = (1/2)\boldsymbol{\omega}^\top \boldsymbol{I}\boldsymbol{\omega} \ge 0$. Taking the time derivative, one arrives at

$$\dot{H} = \boldsymbol{\omega}^\top \boldsymbol{I}\dot{\boldsymbol{\omega}} = \boldsymbol{\omega}^\top(-\boldsymbol{\omega}^\times \boldsymbol{I}\boldsymbol{\omega} + \boldsymbol{u}) = \boldsymbol{\omega}^\top \boldsymbol{u} \tag{36}$$

Integrating both sides gives

$$\int_0^T \boldsymbol{\omega}^\top \boldsymbol{u}\,\mathrm{d}t = H(T) - H(0) \ge -H(0) \tag{37}$$

Hence, $\mathcal{G}_E$ is passive. □

The finite-gain characteristic of $\mathcal{G}_E$ with a prewrap term is guaranteed by the following theorem.

Theorem 2: The new map from the input $\boldsymbol{u}$ to the output $\boldsymbol{\omega}$ has finite gain when adding a prewrap term $-\xi\boldsymbol{\omega}$ into Eq. (1):

$$\boldsymbol{I}\dot{\boldsymbol{\omega}} + \boldsymbol{\omega}^\times \boldsymbol{I}\boldsymbol{\omega} = -\xi\boldsymbol{\omega} + \boldsymbol{u} \tag{38}$$

where $\xi > 0$ is an arbitrary small number.

Proof: Rewrite Eq. (38) like

$$\boldsymbol{I}\dot{\boldsymbol{\omega}} + \boldsymbol{\omega}^\times \boldsymbol{I}\boldsymbol{\omega} + \xi\boldsymbol{\omega} = \boldsymbol{u} \tag{39}$$

Multiply both sides of Eq. (39) with $\boldsymbol{\omega}^\top$, and it becomes

$$\boldsymbol{\omega}^\top \boldsymbol{I}\dot{\boldsymbol{\omega}} + \boldsymbol{\omega}^\top\boldsymbol{\omega}^\times \boldsymbol{I}\boldsymbol{\omega} + \xi\boldsymbol{\omega}^\top\boldsymbol{\omega} = \boldsymbol{\omega}^\top \boldsymbol{u} \tag{40}$$

Since $\boldsymbol{\omega}^\top\boldsymbol{\omega}^\times = 0$,

$$\frac{\mathrm{d}}{\mathrm{d}t}\left[\frac{1}{2}\boldsymbol{\omega}^\top \boldsymbol{I}\boldsymbol{\omega}\right] + \xi\boldsymbol{\omega}^\top\boldsymbol{\omega} = \boldsymbol{\omega}^\top \boldsymbol{u} \tag{41}$$

As depicted in Fig. 9, the error vector is defined as $\boldsymbol{e} = -\xi\boldsymbol{\omega} + \boldsymbol{u}$. According to Lemma 1, the passivity of $\mathcal{G}_E$ leads to

$$\int_0^T \boldsymbol{\omega}^\top \boldsymbol{e}\,\mathrm{d}t = \int_0^T \boldsymbol{\omega}^\top(-\xi\boldsymbol{\omega} + \boldsymbol{u})\,\mathrm{d}t \ge 0 \tag{42}$$

Then

$$\int_0^T \boldsymbol{\omega}^\top \boldsymbol{u}\,\mathrm{d}t \ge \xi\int_0^T \boldsymbol{\omega}^\top\boldsymbol{\omega}\,\mathrm{d}t \tag{43}$$

This implies that the system shown in Eq. (38) will maintain passivity from input $\boldsymbol{u}$ to output $\boldsymbol{\omega}$. Using the Cauchy–Schwarz inequality, we have

$$\int_0^T \boldsymbol{\omega}^\top \boldsymbol{u}\,\mathrm{d}t \le \left(\int_0^T \boldsymbol{\omega}^\top\boldsymbol{\omega}\,\mathrm{d}t\right)^{1/2}\left(\int_0^T \boldsymbol{u}^\top\boldsymbol{u}\,\mathrm{d}t\right)^{1/2} \tag{44}$$

Substituting Eq. (43) into Eq. (44), we can get

$$\xi\int_0^T \boldsymbol{\omega}^\top\boldsymbol{\omega}\,\mathrm{d}t \le \left(\int_0^T \boldsymbol{\omega}^\top\boldsymbol{\omega}\,\mathrm{d}t\right)^{1/2}\left(\int_0^T \boldsymbol{u}^\top\boldsymbol{u}\,\mathrm{d}t\right)^{1/2} \tag{45}$$

This implies that

$$\xi\left(\int_0^T \boldsymbol{\omega}^\top\boldsymbol{\omega}\,\mathrm{d}t\right)^{1/2} \le \left(\int_0^T \boldsymbol{u}^\top\boldsymbol{u}\,\mathrm{d}t\right)^{1/2} \tag{46}$$

Letting $T \to \infty$ and assuming $\boldsymbol{u} \in \mathcal{L}_2$, one has

$$\|\boldsymbol{\omega}\|_2 \le \xi^{-1}\|\boldsymbol{u}\|_2 \tag{47}$$

which means

$$\|\mathcal{G}_E\|_2 = \sup_{0\neq\boldsymbol{u}\in\mathcal{L}_2}\frac{\|\boldsymbol{\omega}\|_2}{\|\boldsymbol{u}\|_2} \le \frac{1}{\xi} \tag{48}$$

□

C. Controller Synthesis

Consider a controller

$$\dot{\boldsymbol{x}}_c = \boldsymbol{A}_c\boldsymbol{x}_c + \boldsymbol{B}_c\boldsymbol{u}_c, \qquad \boldsymbol{y}_c = \boldsymbol{C}_c\boldsymbol{x}_c \tag{49}$$

where $\boldsymbol{x}_c$ is the controller's state, and $\boldsymbol{y}_c$ is the controller's output. The control block is illustrated in Fig. 10. Because of the negative feedback connection, $\boldsymbol{y}_c = -\boldsymbol{u}$ and $\boldsymbol{y} = \boldsymbol{u}_c$. Given that the Euler's equation with the prewrap term is a passive system and has a finite gain, it can be stabilized by interconnecting a strict passive controller as a negative feedback, which is stated in the passivity theorem [26]. A strictly passive controller is provided by the next lemma.

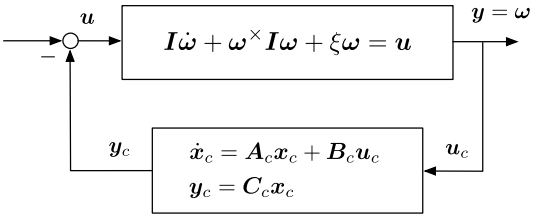

Fig. 10 Control block.

Lemma 2 (KYP lemma): Consider a system given in Eq. (49) as $G_c(s) = C_c(s\mathbf{1} - A_c)^{-1}B_c$. The matrices A_c, B_c, C_c form a minimal state-space realization. Assuming that A_c is Hurwitz, this system is SPR if and only if there are real matrices $P_c = P_c^{\top} > 0$ and $Q_c = Q_c^{\top} > 0$ that satisfy the conditions

$$\begin{aligned} P_c A_c + A_c^{\top} P_c &= -Q_c \\ P_c B_c &= C_c^{\top} \end{aligned} \tag{50}$$

For a proof, see [27]. If $G_c(s) = C_c(s\mathbf{1} - A_c)^{-1}B_c + \mu\mathbf{1}$ for an arbitrarily small $\mu > 0$, the SPR system $G_c(s)$ corresponds to a strictly passive system with finite gain.

To synthesize the controller, Eq. (38) can be linearized via the small angle and rate assumption $\boldsymbol{\omega} \doteq \dot{\boldsymbol{\theta}}$ as follows:

$$\begin{bmatrix} \dot{\theta} \\ \ddot{\theta} \end{bmatrix} = \underbrace{\begin{bmatrix} \mathbf{0} & \mathbf{1} \\ \mathbf{0} & -I^{-1}\xi \end{bmatrix}}_{A_l} \underbrace{\begin{bmatrix} \theta \\ \dot{\theta} \end{bmatrix}}_{x_l} + \underbrace{\begin{bmatrix} \mathbf{0} \\ I^{-1} \end{bmatrix}}_{B_l} u, \quad y_l = \underbrace{\begin{bmatrix} \mathbf{0} & \mathbf{1} \end{bmatrix}}_{C_l} \begin{bmatrix} \theta \\ \dot{\theta} \end{bmatrix} \tag{51}$$

Following the algorithm in [28], the matrix C_c can be formulated as a state-feedback gain from the linear quadratic regulator (LQR) algorithm with suitable selection of the weight matrices $\hat{Q} = \hat{Q}^{\top} > 0$ and $R = R^{\top} > 0$ along with the matrices B_l and C_l in Eq. (51). A Hurwitz matrix $A_c = A_l - B_l C_c$ is obtained. Then, the matrices P_c and B_c can be obtained from Eq. (50) with a suitable selection of $Q_c = Q_c^{\top} > 0$. Hence, the standard KYP lemma generates an SPR controller $G_{c,\mathrm{KYP}}(s) = C_c(s\mathbf{1} - A_c)^{-1}B_c$.

This synthesis process is conducted in the time domain. Therefore, it can maintain passivity over the entire frequency range. Considering the energy migration from the low- to high-frequency ranges, it is supposed that a hybrid frequency controller might be more effective than $G_{c,\mathrm{KYP}}(s)$ designed based on the standard KYP lemma. Motivated by this assumption, first, the generalized KYP lemma is taken to design a hybrid passive/finite gain controller for Euler's equation with the prewrap term. Then, this assumption is extended to the spacecraft attitude control problem in which quaternions are taken into account with the prewrap Euler's equation.

1. Case A: Hybrid Passive/Finite Gain Controller for the Prewrap Euler's Equation

In this case, the entire frequency range is split by the critical frequency ω_c into two parts, which are low- and high-frequency ranges. The approach to formulate the matrices A_c and B_c is consistent with those in the synthesis of $G_{c,\mathrm{KYP}}(s)$. The controller's output gain C_c in Eq. (49) is renamed as K. The hybrid frequency controller is denoted by $G_{c2}(s) = K(s\mathbf{1} - A_c)^{-1}B_c$. The formula of the matrix K involves the hybrid passive/finite gain theorem and the GKYP lemma, which is given as follows.

Lemma 3 (GKYP lemma [20]): Consider the system $G(s) = C(s\mathbf{1} - A)^{-1}B$ and a given matrix $\Pi = \Pi^{\mathrm{H}}$. The following two statements are equivalent:

1) Frequency domain condition:

$$\begin{bmatrix} G(\mathrm{j}\omega) \\ \mathbf{1} \end{bmatrix}^{\mathrm{H}} \Pi \begin{bmatrix} G(\mathrm{j}\omega) \\ \mathbf{1} \end{bmatrix} < 0 \tag{52}$$

2) Linear matrix inequality: There are two matrices, $P = P^{\top}$ and $Q = Q^{\top} \geq 0$, such that

$$\begin{bmatrix} A & B \\ \mathbf{1} & \mathbf{0} \end{bmatrix}^{\mathrm{H}} L(P,Q) \begin{bmatrix} A & B \\ \mathbf{1} & \mathbf{0} \end{bmatrix} + \begin{bmatrix} C & \mathbf{0} \\ \mathbf{0} & \mathbf{1} \end{bmatrix}^{\mathrm{H}} \Pi \begin{bmatrix} C & \mathbf{0} \\ \mathbf{0} & \mathbf{1} \end{bmatrix} < 0 \tag{53}$$

Here, the function $L(P,Q)$ depends on the matrices P and Q. It has particular forms in different frequency ranges, which is described below.

Following Theorem 1, the controller G_{c2} is SPR over $-\omega_c \leq \omega \leq \omega_c$ when Eq. (34) is satisfied. The equivalent form of the GKYP lemma uses

$$\Pi = \begin{bmatrix} \mathbf{0} & -\mathbf{1} \\ -\mathbf{1} & \mathbf{0} \end{bmatrix}, \qquad L(P,Q) = \begin{bmatrix} -Q & P \\ P & \omega_c^2 Q \end{bmatrix}$$

in Eq. (53). Hence, the controller G_{c2} has passivity over $-\omega_c \leq \omega \leq \omega_c$ when the following inequality is satisfied:

$$\begin{bmatrix} A_c & B_c \\ \mathbf{1} & \mathbf{0} \end{bmatrix}^{\mathrm{H}} \begin{bmatrix} -Q_l & P_l \\ P_l & \omega_c^2 Q_l \end{bmatrix} \begin{bmatrix} A_c & B_c \\ \mathbf{1} & \mathbf{0} \end{bmatrix} + \begin{bmatrix} K & \mathbf{0} \\ \mathbf{0} & \mathbf{1} \end{bmatrix}^{\mathrm{H}} \begin{bmatrix} \mathbf{0} & -\mathbf{1} \\ -\mathbf{1} & \mathbf{0} \end{bmatrix} \begin{bmatrix} K & \mathbf{0} \\ \mathbf{0} & \mathbf{1} \end{bmatrix} < 0 \tag{54}$$

where $P_l = P_l^{\top}$ and $Q_l = Q_l^{\top} > 0$. The variables in the LMI are K, P_l, and Q_l.

In the high-frequency range $|\omega| > \omega_c$, the gain γ_2 of the controller G_{c2} should be finite, which implies that the controller system is bounded real. Because the prewrap Euler's equation has finite gain $\gamma_1 \leq 1/\xi$, the gain γ_2 of the controller G_{c2} is determined as $\gamma_2 < \xi$ in Theorem 1. The equivalent bounded-real form of the GKYP lemma over $|\omega| > \omega_c$ is obtained by substituting

$$\Pi = \begin{bmatrix} \mathbf{1} & \mathbf{0} \\ \mathbf{0} & -\gamma_2^2\mathbf{1} \end{bmatrix}, \qquad L(P,Q) = \begin{bmatrix} Q & P \\ P & -\omega_c^2 Q \end{bmatrix}$$

into Eq. (53) to yield

$$\begin{bmatrix} A_c & B_c \\ \mathbf{1} & \mathbf{0} \end{bmatrix}^{\mathrm{H}} \begin{bmatrix} Q_h & P_h \\ P_h & -\omega_c^2 Q_h \end{bmatrix} \begin{bmatrix} A_c & B_c \\ \mathbf{1} & \mathbf{0} \end{bmatrix} + \begin{bmatrix} K & \mathbf{0} \\ \mathbf{0} & \mathbf{1} \end{bmatrix}^{\mathrm{H}} \begin{bmatrix} \mathbf{1} & \mathbf{0} \\ \mathbf{0} & -\gamma_2^2\mathbf{1} \end{bmatrix} \begin{bmatrix} K & \mathbf{0} \\ \mathbf{0} & \mathbf{1} \end{bmatrix} < 0 \tag{55}$$

The Schur complement is used to transform Eq. (55) into

$$\begin{bmatrix} A_c^{\top} Q_h A_c + P_h A_c + A_c^{\top} P_h - \omega_c^2 Q_h & A_c^{\top} Q_h B_c + P_h B_c & K^{\top} \\ \mathrm{sym} & B_c^{\top} Q_h - \gamma_2^2 \mathbf{1} & \mathbf{0} \\ \mathrm{sym} & \mathrm{sym} & -\mathbf{1} \end{bmatrix} < 0 \tag{56}$$

which does not contain a nonlinear term with respect to K in Eq. (55). The matrices K, $P_h = P_h^{\top}$, and $Q_h = Q_h^{\top} > 0$ are the variables in the LMI (56).

The hybrid controller G_{c2} is SPR in the low-frequency range and has finite gain in the high-frequency range if the gain K satisfied LMIs (54) and (56). However, a feasible solution of LMIs (54) and (56) might not be unique. We take an optimization approach to find an exclusive K. An appropriate objective function is set as

$$\mathcal{J} = \mathrm{tr}[(K - C_c)(K - C_c)^{\top}] \tag{57}$$

This objective function will produce a controller designed with the GKYP lemma to mimic the controller from the standard KYP lemma but also one with small high-frequency gain γ_2.

Using a similar approach as [18] for solving the LMIs, an additional variable $\boldsymbol{Z} = \boldsymbol{Z}^{\top} \geq 0$ is introduced, and two additional constraints are employed as

$$\text{tr}[\boldsymbol{Z}] \leq \mathcal{J} \tag{58a}$$

$$(\boldsymbol{K} - \boldsymbol{C}_c)(\boldsymbol{K} - \boldsymbol{C}_c)^{\top} \leq \boldsymbol{Z} \tag{58b}$$

These additional constraints are logical since minimal $\mathcal{J}$ implies minimal tr[$\boldsymbol{Z}$] as $(\boldsymbol{K} - \boldsymbol{C}_c)(\boldsymbol{K} - \boldsymbol{C}_c)^{\top}$ is being minimized. Because the left-hand side of Eq. (58b) is nonlinear in $\boldsymbol{K}$, the Schur complement is used to transform it as

$$-\begin{bmatrix} \boldsymbol{Z} & (\boldsymbol{K} - \boldsymbol{C}_c)^{\top} \\ \text{sym} & \boldsymbol{1} \end{bmatrix} \leq 0 \tag{59}$$

The optimal gain $\boldsymbol{K}$ can be determined from following optimization problem:

$$\begin{array}{ll} \min & \mathcal{J}(\boldsymbol{K}, \boldsymbol{P}_l, \boldsymbol{Q}_l, \boldsymbol{P}_h, \boldsymbol{Q}_h, \boldsymbol{Z}) \\ \text{subject to} & \text{LMIs in (54), (56), (59)} \end{array} \tag{60}$$

Up to here, a hybrid SPR/finite gain controller $\boldsymbol{G}_{c2} = \boldsymbol{K}(s\boldsymbol{1} - \boldsymbol{A}_c)^{-1}\boldsymbol{B}_c$ has been accomplished using the GKYP lemma and the optimization. The recipe for synthesis of the controller $\boldsymbol{G}_{c2}(s)$ is given in Algorithm 2.

Algorithm 2: Steps to synthesize controller $\boldsymbol{G}_{c2}(s) = \boldsymbol{K}(s\boldsymbol{1} - \boldsymbol{A}_c)^{-1}\boldsymbol{B}_c$

1: Form the linear plant model $\boldsymbol{G}_{c1}(s) = \boldsymbol{C}_l(s\boldsymbol{1} - \boldsymbol{A}_l)^{-1}\boldsymbol{B}_l$ where $\boldsymbol{A}_l$, $\boldsymbol{B}_l$, and $\boldsymbol{C}_l$ are given in Eq. (51).

2: Formulate $\boldsymbol{C}_c$ as a state-feedback gain from the LQR algorithm with suitable selection $\bar{\boldsymbol{Q}} = \bar{\boldsymbol{Q}}^{\top} > 0$ and $\boldsymbol{R} = \boldsymbol{R}^{\top} > 0$ along with the matrices $\boldsymbol{A}_l$, $\boldsymbol{B}_l$, and $\boldsymbol{C}_l$ in Eq. (51).

3: Calculate $\boldsymbol{B}_c$ from Eq. (50) with a suitable selection of $\boldsymbol{Q}_c = \boldsymbol{Q}_c^{\top} > 0$.

4: Calculate $\boldsymbol{A}_c$ from $\boldsymbol{A}_c = \boldsymbol{A}_l - \boldsymbol{B}_l\boldsymbol{C}_c$, where $\boldsymbol{A}_l$ and $\boldsymbol{B}_l$ are formed from Eq. (51).

5: Determine gain $\boldsymbol{K}$ by solving the optimization problem shown in Eq. (60). [The problem shown in Eq. (60) must satisfy Eq. (54) and Eq. (56), which are derived from the GKYP lemma in frequency domain. The controller $\boldsymbol{G}_{c2}(s)$ will maintain passivity in the low-frequency range and has small finite gain in the high-frequency range.]

Remark 3: Note that Algorithm 2 produces a controller with passive characteristics at low frequency (i.e., $\boldsymbol{G}_{c2}(\text{j}\omega) + \boldsymbol{G}_{c2}^{\text{H}}(\text{j}\omega) \geq 0, \omega \leq \omega_c$) and small gain at high frequency (i.e., $\boldsymbol{G}_{c2}^{\text{H}}(\text{j}\omega)\boldsymbol{G}_{c2}(\text{j}\omega) \leq \gamma_2^2\boldsymbol{1}$, $\omega > \omega_c$). These two characteristics are facilitated by the GKYP lemma with the two LMIs in Eqs. (54) and (56).

Remark 4: For the controller $\boldsymbol{G}_{c2}$, we use a linear model of the plant to design a linear controller. However, the hybrid passivity/finite gain theorem in Theorem 1 guarantees that it will stabilize the original nonlinear system.

Remark 5: As a competitive controller, $\boldsymbol{G}_{c,\text{KYP}}$ is formulated using the KYP lemma in the time domain. Its frequency domain properties cannot be manipulated directly. However, the frequency domain properties of the controller $\boldsymbol{G}_{c2}$ are determined by the GKYP lemma [i.e., Eq. (54) and Eq. (56)]. The selection of a small value of γ_2 in Eq. (56) enables $\boldsymbol{G}_{c2}$ to accommodate the energy transfer phenomenon in the high-frequency domain.

The moment of inertia $\boldsymbol{I}$ and the initial values of the angular velocities are set as the same as those in Sec. III. The weights of the LQR algorithm are set as $\bar{\boldsymbol{Q}} = 3.3 \times \text{diag}\{1, 1, 1, 10, 10, 10\}$, $\boldsymbol{Q}_c = 20 \times \text{diag}\{1, 1, 1, 10, 10, 10\}$, and $\boldsymbol{R} = 2.3 \times \boldsymbol{1}$, where $\boldsymbol{1}$ is an identity matrix with suitable size required by the LQR algorithm. The prewrap parameter in Eq. (38) is set as $\xi = 0.01$. The critical frequency is $\omega_c = 6$ rad/s. Figure 11 shows the time response of the angular velocities under the controllers $\boldsymbol{G}_{c,\text{KYP}}$ and $\boldsymbol{G}_{c2}$, respectively. The performance under the controller $\boldsymbol{G}_{c2}$ is better than that under the controller $\boldsymbol{G}_{c,\text{KYP}}$. From Fig. 12, the control inputs from $\boldsymbol{G}_{c2}$ are smaller than those from $\boldsymbol{G}_{c,\text{KYP}}$. Figure 13 illustrates the frequency responses of the maximum singular value of $\boldsymbol{G}_{c,\text{KYP}}(\text{j}\omega)$ and $\boldsymbol{G}_{c2}(\text{j}\omega)$, where the maximum singular value of $\boldsymbol{G}(\text{j}\omega)$ is defined as $\bar{\sigma}(\boldsymbol{G}(\text{j}\omega)) = \sqrt{\bar{\lambda}[\boldsymbol{G}^{\text{H}}(\text{j}\omega)\boldsymbol{G}(\text{j}\omega)]}$ when $\lambda[\star]$ are the eigenvalues of a matrix $[\star]$. At the low-frequency ranges, the gain of the controller $\boldsymbol{G}_{c2}$ is larger than that from the controller $\boldsymbol{G}_{c,\text{KYP}}$ and becomes smaller than that from the controller $\boldsymbol{G}_{c,\text{KYP}}$ in the high-frequency ranges. This feature can lead the low-frequency components of the state to decay to equilibrium faster. Moreover, the high-frequency components are applied with lower gains, which means that less control efforts are consumed. The special consideration to accommodate energy transfer for the high-frequency domain in the control scheme is effective.

2. *Case B: Hybrid Passive/Finite Gain Controller for the Spacecraft Attitude Control Problem*

From the above simulation results, it is intuitive to suppose that the controller $\boldsymbol{G}_{c2} = \boldsymbol{K}(s\boldsymbol{1} - \boldsymbol{A}_c)^{-1}\boldsymbol{B}_c$ might be still more efficient on the spacecraft attitude control problem than the controller based on the standard KYP lemma when quaternions are also taken into consideration. As for the spacecraft attitude control, the quaternions $[\boldsymbol{\epsilon}, \eta]$ are selected as attitude parameters to describe the rotation of the spacecraft. The kinematic equations of a rigid-body spacecraft are given by

$$\dot{\boldsymbol{\epsilon}} = \frac{1}{2}(\eta\boldsymbol{1} + \boldsymbol{\epsilon}^{\times})\boldsymbol{\omega}, \qquad \dot{\eta} = -\frac{1}{2}\boldsymbol{\epsilon}^{\top}\boldsymbol{\omega} \tag{61}$$

For the prewrap Euler's equation and the quaternions kinematic equation, consider a new controller

$$\boldsymbol{u}_n = \boldsymbol{u}_p + \boldsymbol{u} \tag{62}$$

where $\boldsymbol{u}_p = -k\boldsymbol{\epsilon}(k > 0)$. The other part $\boldsymbol{u}$ is formulated as almost same as the controller design in case A except the linearized form of Eq. (38) when Eq. (62) is substituted into Eq. (38) and then linearized as

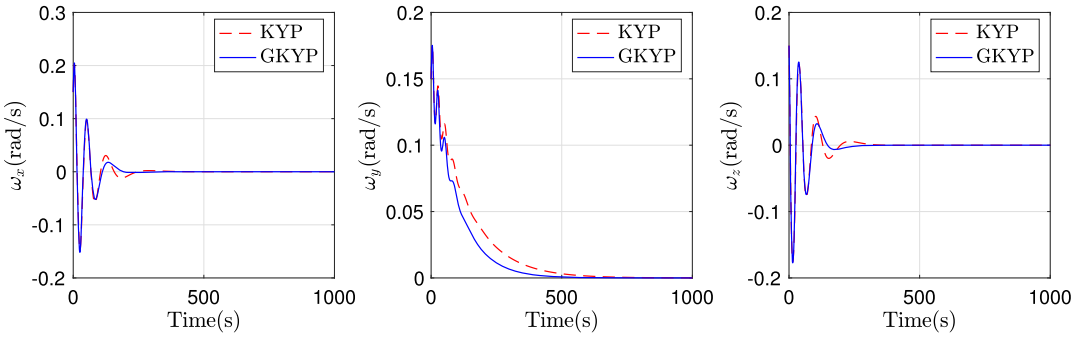

Fig. 11 Time response of $\boldsymbol{\omega}$.

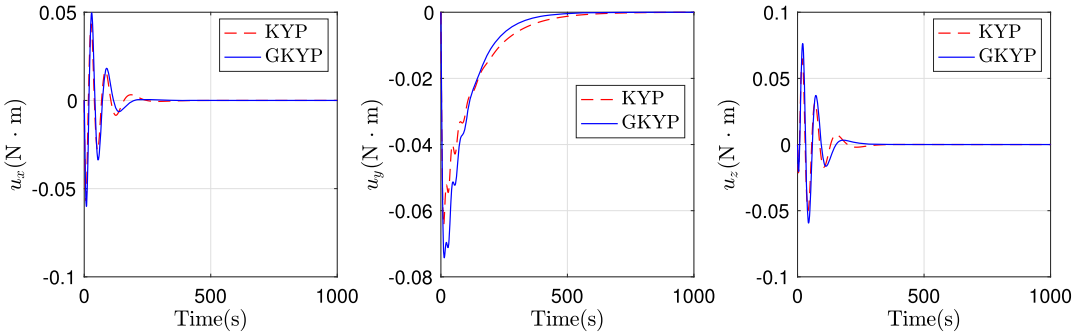

Fig. 12 Time response of $\boldsymbol{u}$.

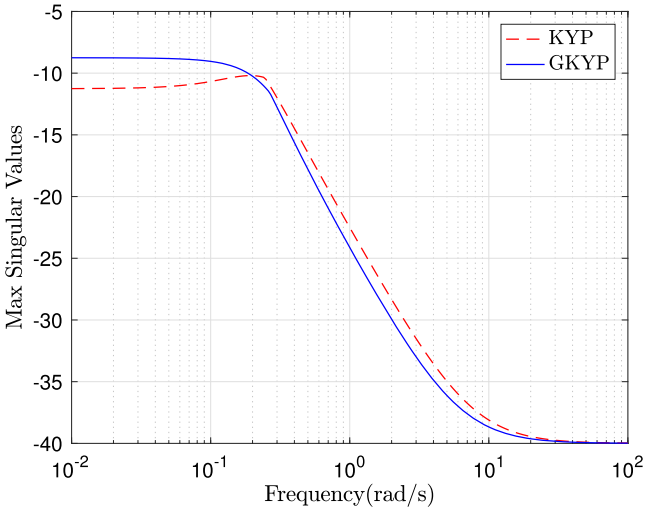

Fig. 13 Maximum singular values of two controllers.

$$\underbrace{\begin{bmatrix}\dot{\boldsymbol{\theta}}\\ \ddot{\boldsymbol{\theta}}\end{bmatrix}=\begin{bmatrix}\mathbf{0} & \mathbf{1}\\ -\boldsymbol{I}^{-1}\left(\frac{k}{2}\right) & -\boldsymbol{I}^{-1}\xi\end{bmatrix}}_{\boldsymbol{A}_l}\underbrace{\begin{bmatrix}\boldsymbol{\theta}\\ \dot{\boldsymbol{\theta}}\end{bmatrix}}_{\boldsymbol{x}_l}+\underbrace{\begin{bmatrix}\mathbf{0}\\ \boldsymbol{I}^{-1}\end{bmatrix}}_{\boldsymbol{B}_l}\boldsymbol{u},\quad \boldsymbol{y}_l=\underbrace{[\mathbf{0}\ \ \mathbf{1}]}_{\boldsymbol{C}_l}\begin{bmatrix}\boldsymbol{\theta}\\ \dot{\boldsymbol{\theta}}\end{bmatrix} \tag{63}$$

All parameters are the same as those in case A except that the controller parameters in the LQR algorithm are changed as $\bar{\boldsymbol{Q}} = 0.8 \times \text{diag}\{1, 1, 1, 10, 10, 10\}$, $\boldsymbol{Q}_c = 2 \times \text{diag}\{1, 1, 1, 10, 10, 10\}$, and $\boldsymbol{R} = 2.3 \times \mathbf{1}$. The initial values of the quaternions are selected as $\boldsymbol{\epsilon}_0 = [-0.5, 0.5, 0.5]^\top$, $\eta_0 = -0.5$. The proportional constant in the controller $\boldsymbol{u}_p$ is set as $k = 0.1$ N · m. Figure 14 indicates the time response of the angular velocities. The time responses of control efforts are shown in Fig. 15. Figure 16 depicts the time response of the quaternions. Compared with Fig. 13, in this case, both controllers' gains are different from case A as displayed in Fig. 17. At the low-frequency range, the angular velocities will converge to zero quickly. At the high-frequency range, the gain from the controller $\boldsymbol{G}_{c2}$ is still smaller than that from the controller $\boldsymbol{G}_{c,\text{KYP}}$. The proposed hybrid

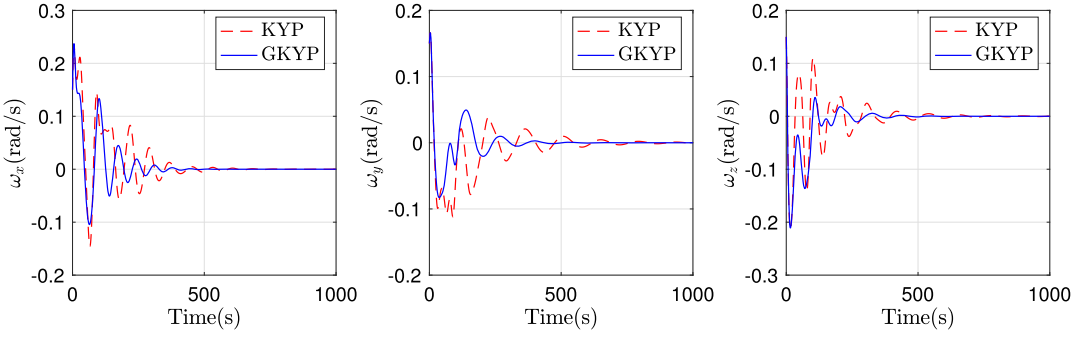

Fig. 14 Time response of $\boldsymbol{\omega}$.

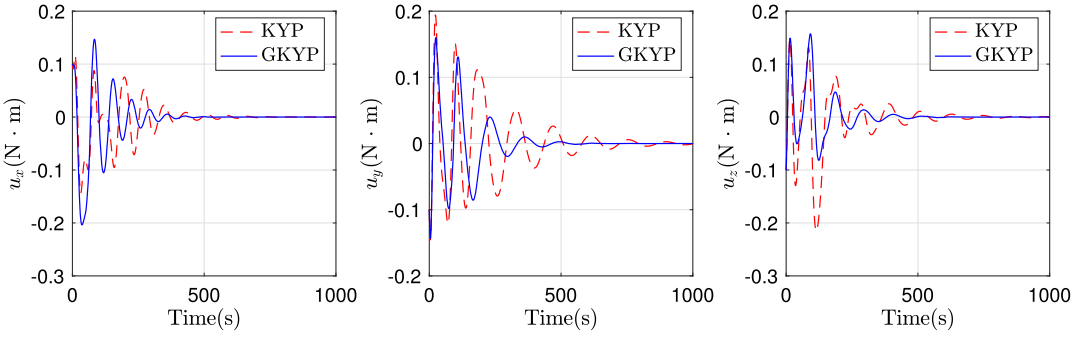

Fig. 15 Time response of $\boldsymbol{u}$.

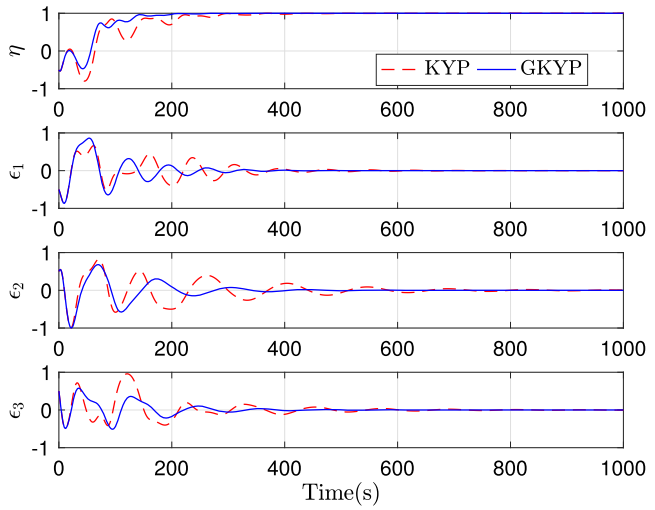

Fig. 16 Time response of quaternions.

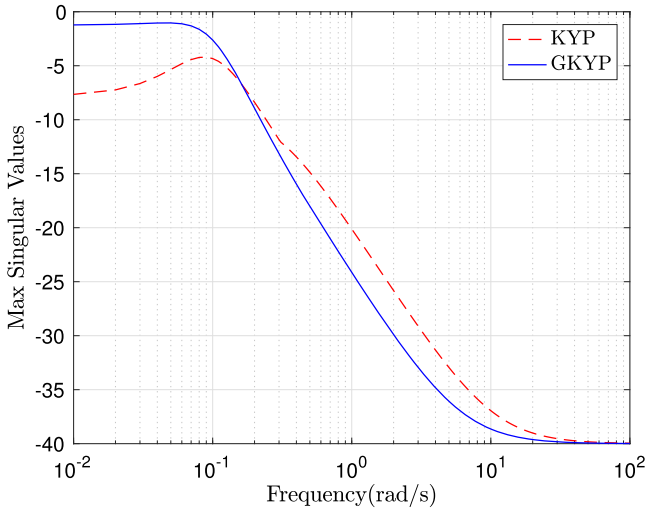

Fig. 17 Maximum singular values of two controllers.

frequency controller for the spacecraft attitude control problem is still effective.

Remark 6: As mentioned in [9], the NOFRFs $\{G_p\}$ yielded by the numerical algorithm depend on the property of the nonlinear system as well as the frequency of the input signals. Besides, the energy transfer property is obtained from the open-loop situation, which might not be equivalent to the closed-loop case. However, in Euler's equation's case, the output's frequency has three possibilities: the energy is transferring to the lower frequency domain, remaining at the same frequency as the inputs, or migrating to the higher frequency domain. The results of the NOFRFs $\{G_p\}$ show that the energy from the low-frequency inputs would transfer to the higher frequency ranges in the outputs, which is the worst case. The hybrid frequency control is motivated by this worst case to guarantee the stability of the closed-loop system and the effectiveness of the controller.

VI. Conclusions

The first contribution of this paper is the solution of Euler's equation using the Volterra series as presented in the frequency domain. The nonlinear behavior of Euler's equation is analyzed by formulating its NOFRFs to show the difference between the input frequencies and the output frequencies, which shows the energy transfer from the low- to high-frequency ranges. A hybrid passive/finite gain frequency controller based on the GKYP lemma has been implemented on Euler's equation to stabilize angular velocities. Compared with the controller based on the KYP lemma, this hybrid frequency controller is more efficient because its gain is larger in the low-frequency ranges, which can drive the angular velocities to equilibrium points with less time. The gain of hybrid controller becomes smaller in the high-frequency ranges, which can accommodate the energy transferred from the low-frequency ranges and consume less energy to achieve similar performance. This feature still remains in the hybrid frequency controller for the attitude control of spacecraft when quaternion feedback is added to the hybrid frequency controller. The effectiveness of the proposed controllers is validated by numerical simulations.

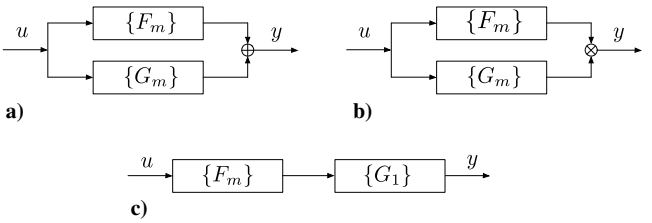

Fig. A1 Interconnection of two systems with a) sum, b) product, and c) cascade.

Appendix : Interconnections of Volterra Kernels [8]

Consider that $\{F_m\}$ and $\{G_m\}$ are the Volterra kernels of two systems. Combine these two systems to form a new system using three interconnection manners, which are sum, product, and cascade. The new system's Volterra kernel $\{H_m\}$ is determined as follows:

a) Sum (Fig. A1a):

$$H_m(s_1,\ldots,s_m) = F_m(s_1,\ldots,s_m) + G_m(s_1,\ldots,s_m) \tag{A1}$$

b) Product (Fig. A1b):

$$H_m(s_1,\ldots,s_m) = \sum_{k=1}^{m-1} F_k(s_1,\ldots,s_k)G_{m-k}(s_{k+1},\ldots,s_m) \tag{A2}$$

c) Cascade (Fig. A1c):

$$H_m(s_1,\ldots,s_m) = G_1(s_1+\cdots+s_m)F_m(s_1,\ldots,s_m) \tag{A3}$$

Acknowledgment

The work reported in this paper was supported by the China Scholarship Council.

References

[1] Hughes, P. C., *Spacecraft Attitude Dynamics*, Dover, Mineola, NY, 2004, pp. 105–108.

[2] Benedetto, S., Biglieri, E., and Daffara, R., "Modeling and Performance Evaluation of Nonlinear Satellite Links—A Volterra Series Approach," *IEEE Transactions on Aerospace and Electronic Systems*, Vol. AES-15, No. 4, 1979, pp. 494–507. https://doi.org/10.1109/TAES.1979.308734

[3] Rugh, W. J., *Nonlinear System Theory: The Volterra/Wiener Approach*, Johns Hopkins Univ. Press, Baltimore, MD, 1981, pp. 3–21.

[4] Marzocca, P., Silva, W. A., and Librescu, L., "Nonlinear Open-/Closed-Loop Aeroelastic Analysis of Airfoils via Volterra Series," *AIAA Journal*, Vol. 42, No. 4, 2004, pp. 673–686. https://doi.org/10.2514/1.9552

[5] Baldelli, D. H., Lind, R., and Brenner, M., "Nonlinear Aeroelastic/Aeroservoelastic Modeling by Block-Oriented Identification," *Journal of Guidance, Control, and Dynamics*, Vol. 28, No. 5, 2005, pp. 1056–1064. https://doi.org/10.2514/1.11792

[6] Omran, A. K., and Newman, B., "Piecewise Global Volterra Nonlinear Modeling and Characterization for Aircraft Dynamics," *Journal of Guidance, Control, and Dynamics*, Vol. 32, No. 3, 2009, pp. 749–759. https://doi.org/10.2514/1.40655

[7] Omran, A., and Newman, B., "Analytical Solution of Uniaxial Flight Systems Using Volterra Kernels in Frequency Domain," *Journal of Guidance, Control, and Dynamics*, Vol. 37, No. 4, 2014, pp. 1080–1090. https://doi.org/10.2514/1.58721

[8] Hélie, T., and Laroche, B., "On the Convergence of Volterra Series of Finite Dimensional Quadratic MIMO Systems," *International Journal of Control*, Vol. 81, No. 3, 2008, pp. 358–370. https://doi.org/10.1080/00207170701561401

[9] Lang, Z. Q., and Billings, S. A., "Energy Transfer Properties of Non-Linear Systems in the Frequency Domain," *International Journal of Control*, Vol. 78, No. 5, 2005, pp. 345–362. https://doi.org/10.1080/00207170500095759

[10] Peng, Z., Lang, Z. Q., and Billings, S. A., "Non-Linear Output Frequency Response Functions for Multi-Input Non-Linear Volterra Systems," *International Journal of Control*, Vol. 80, No. 6, 2007, pp. 843–855. https://doi.org/10.1080/00207170601185038

[11] Lang, Z. Q., Billings, S. A., Yue, R., and Li, J., "Output Frequency Response Function of Nonlinear Volterra Systems," *Automatica*, Vol. 43, No. 5, 2007, pp. 805–816. https://doi.org/10.1016/j.automatica.2006.11.013

[12] Wen, J. T., and Kreutz-Delgado, K., "The Attitude Control Problem," *IEEE Transactions on Automatic Control*, Vol. 36, No. 10, 1991, pp. 1148–1162. https://doi.org/10.1109/9.90228

[13] Sharma, R., and Tewari, A., "Optimal Nonlinear Tracking of Spacecraft Attitude Maneuvers," *IEEE Transactions on Control Systems Technology*, Vol. 12, No. 5, 2004, pp. 677–682. https://doi.org/10.1109/TCST.2004.825060

[14] Boškovic, J. D., Li, S. M., and Mehra, R. K., "Robust Adaptive Variable Structure Control of Spacecraft Under Control Input Saturation," *Journal of Guidance, Control, and Dynamics*, Vol. 24, No. 1, 2001, pp. 14–22. https://doi.org/10.2514/2.4704

[15] Luo, W., Chu, Y. C., and Ling, K. V., "Inverse Optimal Adaptive Control for Attitude Tracking of Spacecraft," *IEEE Transactions on Automatic Control*, Vol. 50, No. 11, 2005, pp. 1639–1654. https://doi.org/10.1109/TAC.2005.858694

[16] Forbes, J. R., "Passivity-Based Attitude Control on the Special Orthogonal Group of Rigid-Body Rotations," *Journal of Guidance, Control, and Dynamics*, Vol. 36, No. 6, 2013, pp. 1596–1605. https://doi.org/10.2514/1.59270

[17] Forbes, J. R., "Attitude Control with Active Actuator Saturation Prevention," *Acta Astronautica*, Vol. 107, Feb.–March 2015, pp. 187–195. https://doi.org/10.1016/j.actaastro.2014.10.006

[18] Forbes, J. R., and Damaren, C. J., "Synthesis of Optimal Finite-Frequency Controllers Able to Accommodate Passivity Violations," *IEEE Transactions on Control Systems Technology*, Vol. 21, No. 5, 2013, pp. 1808–1819. https://doi.org/10.1109/TCST.2012.2216268

[19] Iwasaki, T., and Hara, S., "Generalization of Kalman-Yakubovic-Popov Lemma for Restricted Frequency Inequalities," *Proceedings of the 2003 American Control Conference*, Vol. 5, Inst. of Electrical and Electronics Engineers, New York, 2003, pp. 3828–3833. https://doi.org/10.1109/ACC.2003.1240432

[20] Iwasaki, T., and Hara, S., "Generalized KYP Lemma: Unified Frequency Domain Inequalities with Design Applications," *IEEE Transactions on Automatic Control*, Vol. 50, No. 1, 2005, pp. 41–59. https://doi.org/10.1109/TAC.2004.840475

[21] Swain, A., and Billings, S. A., "Generalized Frequency Response Function Matrix for MIMO Non-Linear Systems," *International Journal of Control*, Vol. 74, No. 8, 2001, pp. 829–844. https://doi.org/10.1080/00207170010030144

[22] Worden, K., Manson, G., and Tomlinson, G., "A Harmonic Probing Algorithm for the Multi-Input Volterra Series," *Journal of Sound and Vibration*, Vol. 201, No. 1, 1997, pp. 67–84. https://doi.org/10.1006/jsvi.1996.0746

[23] Lang, Z. Q., and Billings, S. A., "Output Frequency Characteristics of Nonlinear Systems," *International Journal of Control*, Vol. 64, No. 6, 1996, pp. 1049–1067. https://doi.org/10.1080/00207179608921674

[24] Goodwin, G. C., Graebe, S. F., and Salgado, M. E., *Control System Design*, Prentice-Hall, Upper Saddle River, NJ, 2001, pp. 96–97.

[25] Forbes, J. R., and Damaren, C. J., "Hybrid Passivity and Finite Gain Stability Theorem: Stability and Control of Systems Possessing Passivity Violations," *IET Control Theory & Applications*, Vol. 4, No. 9, 2010, pp. 1795–1806. https://doi.org/10.1049/iet-cta.2009.0137

[26] Marquez, H. J., *Nonlinear Control Systems: Analysis and Design*, Wiley, Hoboken, NJ, 2002, pp. 208–211.

[27] Wen, J. T., "Time Domain and Frequency Domain Conditions for Strict Positive Realness," *IEEE Transactions on Automatic Control*, Vol. 33, No. 10, 1988, pp. 988–992. https://doi.org/10.1109/9.7263

[28] Benhabib, R., Iwens, R., and Jackson, R., "Stability of Large Space Structure Control Systems Using Positivity Concepts," *Journal of Guidance, Control, and Dynamics*, Vol. 4, No. 5, 1981, pp. 487–494. https://doi.org/10.2514/3.56100